Science Advances

AAAS

advances.sciencemag.org/cgi/content/full/4/1/e1701798/DC1

Supplementary Materials for

Superresolution and pulse-chase imaging reveal the role of vesicle transport in polar growth of fungal cells

Lu Zhou, Minoas Evangelinos, Valentin Wernet, Antonia F. Eckert, Yuji Ishitsuka, Reinhard Fischer, G. Ulrich Nienhaus, Norio Takeshita

Published 24 January 2018, *Sci. Adv.* **4**, e1701798 (2018)
DOI: 10.1126/sciadv.1701798

The PDF file includes:

Other Supplementary Material for this manuscript includes the following:
(available at advances.sciencemag.org/cgi/content/full/4/1/e1701798/DC1)

- movie S6 (.mov file). Partial comigration of GFP-ChsB and mCherry-RabA.
- movie S7 (.avi file). Pulse-chase imaging of mEosFP*thermo*-ChsB near the hyphal tip in the presence of microtubule drugs (benomyl, 2 μg/ml).
- movie S8 (.avi file). Pulse-chase imaging of mEosFP*thermo*-ChsB near the hyphal tip in the presence of actin-depolymerizing drugs (cytochalasin A, 2 μg/ml).
- movie S9 (.avi file). Pulse-chase imaging of mEosFP*thermo*-ChsB in the hyphal tip region of the cell from the *kinA* deletion strains.
- movie S10 (.avi file). Pulse-chase imaging of mEosFP*thermo*-ChsB in the hyphal tip region of the cell from the *uncA* deletion strains.
- movie S11 (.avi file). Pulse-chase imaging of mEosFP*thermo*-ChsB in the hyphal tip region of the cell from the myoV deletion strains.
- movie S12 (.avi file). Pulse-chase imaging after mEosFP*thermo*-ChsB photoconversion at the hyphal tip of a wild-type cell.
- movie S13 (.avi file). Pulse-chase imaging after mEosFP*thermo*-ChsB photoconversion at the hyphal tip in the presence of microtubule drugs (benomyl, 2 μg/ml).
- movie S14 (.avi file). Pulse-chase imaging after mEosFP*thermo*-ChsB photoconversion at the hyphal tip in the presence of actin-depolymerizing drugs (cytochalasin A, 2 μg/ml).
- movie S15 (.avi file). Pulse-chase imaging after mEosFP*thermo*-ChsB photoconversion at the hyphal tip of a cell from the *uncA* deletion strain.

Supplementary Materials and Methods

Live cell imaging. PALM images were acquired at room temperature on a modified inverted microscope (Axiovert 200, Zeiss) as described previously (*36*). The fluorescent protein mEosFP*thermo* was photoconverted from its green to red emitting forms by a 405-nm laser at low intensity (0 – 50 W/cm²) and simultaneously excited by a 561-nm laser (200 – 400 W/cm²). The fluorescence emission was filtered by a 607/70 band-pass filter (Semrock, New York, NY) and detected by a back-illuminated EMCCD camera (Ixon Ultra X-7759, Andor, Belfast, UK) with a dwell time of 50 ms/frame. Diode-pumped solid-state lasers, with wavelengths 561 nm (Gem 561, Laser Quantum, Konstanz, Germany), 473 nm (LuxX 473-100, Omicron-Laserage Laserprodukte, Rodgau-Dudenhofen, Germany) and 405 nm (Stradus 405-250, Vortran Laser Technology, Sacramento, California USA) were employed for excitation and photoactivation of the fluorophores. All laser beams were combined via dichroic mirrors (AHF, Tübingen, Germany) and passed through an acousto-optical tunable filter (AOTFnC-400.650, A-A, Opto-Electronic, Orsay Cedex, France) to achieve precise laser intensity control at the sample. 8-well chamber slides (VWR, Darmstadt, Germany) were used for cell imaging.

Molecule localization analyses were carried out on a personal computer using an Intel(R) Core(TM) i7-4930K processor clocked at 3.40 GHz with 32.0 GB memory and a NVIDIA GeForce GTX 760 graphics card with 4.0 GB memory, using a-livePALM (*35*), a custom-written analysis software for localization microscopy running under the MATLAB R2015b (The Mathworks, Natick, MA) environment. For cluster analysis (*36*), molecules from 500 continuous frames (25 s) were collected and analyzed. Only molecules with more than 200 registered photons and localization precision <70 nm were used for analysis and rendering. Molecules localized within 100 nm in space and 50 ms in time were considered to be identical and assigned to a weighted value of 1/F (F is number of frames in which a particular molecule can be detected). For each molecule, we computed the number of detected neighboring molecules within 50 nm distance. If one molecule contains more than 10 neighboring molecules, the pixel where the central molecule stands was considered as a cluster pixel. Adjacent cluster pixels were defined as belonging to the same cluster. Include the text, figures, and tables of the Supplementary Materials at the end of your Word manuscript if possible. Include captions for other file types (see below).

Quantitative analysis of the number of photoconverted molecules. To compare the amount of photoconverted proteins in fig. 3A-C, we performed a quantitative intensity analysis of the different strains, focusing on the first frame after photoconversion (at 1 s). In fig. S3A, we have marked the regions in which the local intensities were determined with red ellipses. Importantly, all analyzed images were acquired with similar power of the 405 nm laser (photoconversion) and 561 nm laser (fluorescence excitation). Background was subtracted from the local intensity of each image using ImageJ. For each strain, images of five individual cells were analyzed and the local intensities (camera A/D counts) were averaged (fig. S3B, left axis). Since all measured data were acquired with the same camera setting for imaging, we can convert the local intensity value (A/D count) to the local molecule number. With our a-livePALM software, the photon number of single emitters can be precisely determined. However, because vesicles typically carry multiple mEosFP*thermo*-ChsB molecules (fig. S3C, red spots), the challenge is how to obtain photon numbers of single fluorophores. To this end, we selectively analyzed the last few frames from single vesicles prior to complete photobleaching, which are likely to contain only a single fluorescing mEosFP*thermo*-ChsB molecule (fig. S3C). Because the very last frame contains variable photon numbers because it is unclear at which point during the 50 ms camera exposure time the mEosFP*thermo* photobleaches, we analyzed the fluorescence from the penultimate frame of an individual vesicles. To be even further on the safe side, we selected only those vesicles that can be observed in at least three continuous frames.

We did this analysis with wildtype cells, for which vesicle transport is slower than for the other strains, so they are more easily tracked. We analyzed the images from 30 - 45 s (frames 600 - 900) after photoconversion because most of the mEosFP*thermo* molecules are already bleached in this time interval, leading to a high probability to observe only emission from vesicles containing a single mEosFP*thermo* fluorophore. With a total of 107 events detected from three wildtype cells, we obtained an average number of photons of 184 ± 92 (S.D.) per molecule; the distribution of photon numbers is shown in fig. S3D. The system readout rate and the EM gain of our camera were set to 10 MHz and 150, respectively. With this readout rate, the CCD sensitivity (electrons per A/D count) is 4.61, as given by the camera data sheet. With the average photon number per molecule calculated above, we convert the intensity value (fig. S3B, left vertical axis) to the number of molecules (fig. S3B, right vertical axis). Typically, 500 - 1500 molecules were locally photoconverted by 1 s exposure to the 405 nm laser spot.

qRT-PCR. Fresh conidia were cultivated in minimal medium supplemented with 2 % glycerol for 18 h at 37 °C. The mycelium was harvested and frozen immediately in liquid nitrogen. To isolate RNA, we used the E.Z.N.A Fungal RNA Kit (OMEGA bio-tek, Norcross, USA) according to the manufacturer's protocol. To remove DNA, the RNA was treated with TURBO DNA-free kit (Thermo Fisher, Waltham, USA) and diluted to 50 ng/µl with DEPC water. Quantitative real-time PCR (qRT-PCR) was performed using SensiFASt SYBR and Fluorescein One-Step kit (Bioline, London, UK). Each reaction was carried out with 0.2 µM primer and 100 ng RNA in a total volume of 25 µl. To amplify the *chsB* gene, we used the primer set, chsb-RT-f: 5'-CTGGCGAGCATACTTATGATG-3' and chsb-RT-r: 5'-TAAGGCCACGCTGCTGATG-3'. For normalization of the expression, the histone 2b gene was used, and each reported expression level was averaged over three biological and technical replicates.

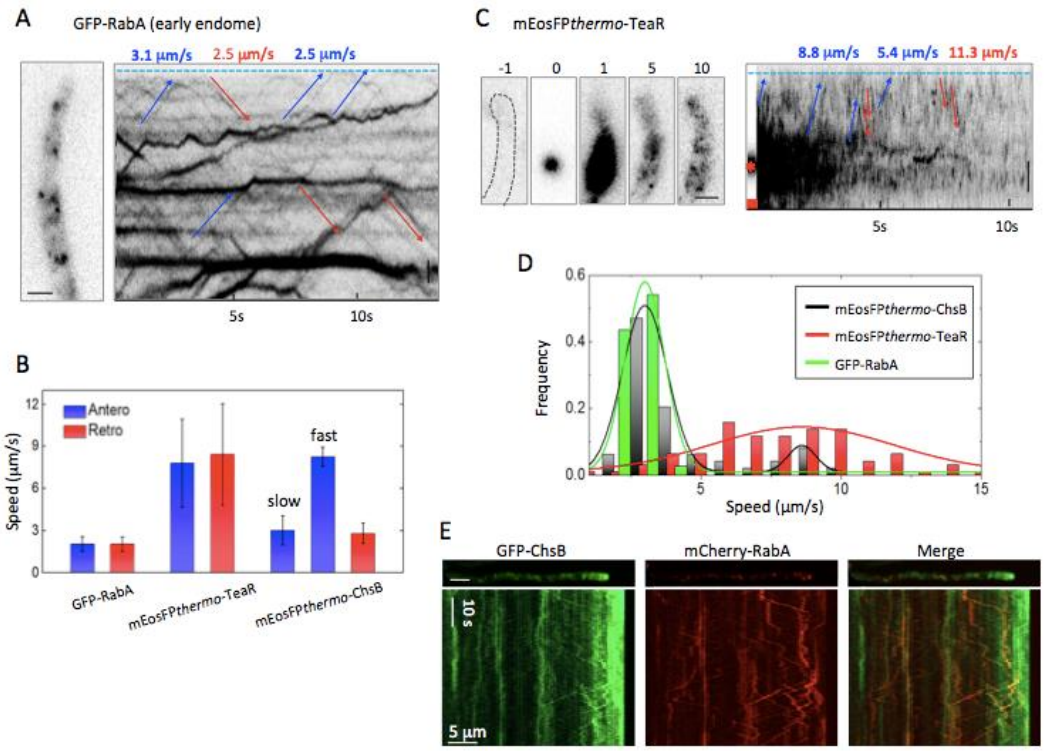

fig. S1. Transport of EEs and SVs. (A) Left: image, right: kymograph of GFP-RabA movement in a wildtype cell; see corresponding Movie S4. Arrows indicate anterograde (blue) and retrograde (red) transport. (B) Speed of anterograde (blue) and retrograde (red) transport of GFP-RabA, mEosFP*thermo*-TeaR and mEosFP*thermo*-ChsB (mean ± SD). (C) Left: Image sequence, right: kymograph of mEosFP*thermo*-TeaR, see corresponding Movie S5. Arrows mark anterograde (blue) and retrograde (red) transport events. Vertical and horizontal scale bars (A and C), 2 µm. The elapsed time is given in seconds (A and C). (D) Speed distributions of anterograde transport of GFP-RabA, mEosFP*thermo*-TeaR and mEosFP*thermo*-ChsB. (E) Kymographs from Movie S6. Vertical and horizontal scale bars, 5 µm and 10 s.

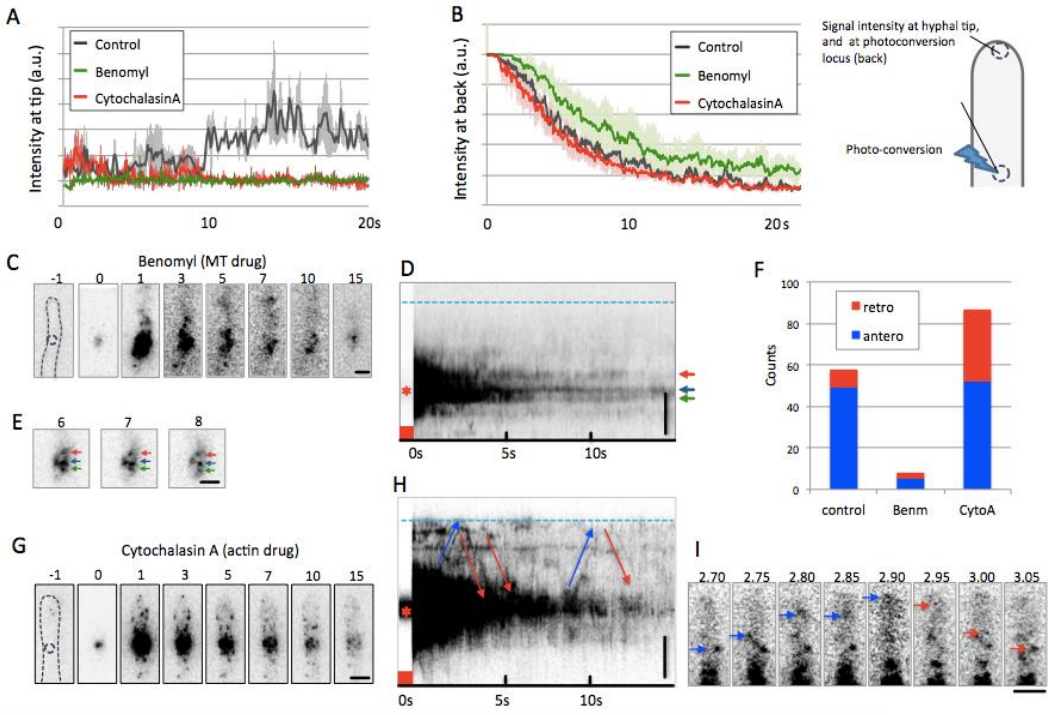

fig. S2. Pulse-chase analysis of mEosFP*thermo*-ChsB near the hyphal tip in the presence of microtubule or actin-depolymerizing drugs. (A and B) Time courses of signal intensity at (A) the hyphal tip and (B) the photoconversion locus from the control (black), with benomyl (green) and with cytochalasin A (red), calculated from the corresponding kymographs and shown as mean ± SD, n = 3-5. (C) Image sequences upon photoconversion in a spot ~5 µm behind the hyphal tip (dashed circle in panel '–1') in the presence of benomyl (2 µg/ml); photoconverting 405-nm light was applied at t = 0 s for 1 s. The elapsed time is given in seconds. (D) Kymograph from the image sequence shown in panel (C); arrows point to immobile spots. The blue dashed line and the asterisk mark the positions of the hyphal tip and the photoconversion locus, respectively; the red square indicates the photoconversion interval. Vertical scale bar, 2 µm. (E) Image sequences of immobile spots for the time interval 6 – 8 s. (F) Number of anterograde (blue) or retrograde (red) transport events in 20 kymographs from the control, and in the presence of benomyl or cytochalasin A. (G) Image sequences upon photoconversion in a spot ~5 µm behind the hyphal tip in the presence of cytochalasin A (2 µg/ml). Photoconverting 405-nm light was applied at t = 0 s for 1 s; the elapsed time is given in seconds. (H) Kymograph from the image sequence shown in panel (G). Arrows indicate anterograde (blue) and retrograde (red) transport events. The blue dashed line and the asterisk mark the positions of the hyphal tip and the photoconversion locus, respectively; the red square indicates the photoconversion interval. Vertical scale bar, 2 µm. (I) Image sequences of anterograde and retrograde transport from 2.7 – 3.05 s. Scale bars (C, E, G, I), 2 µm.

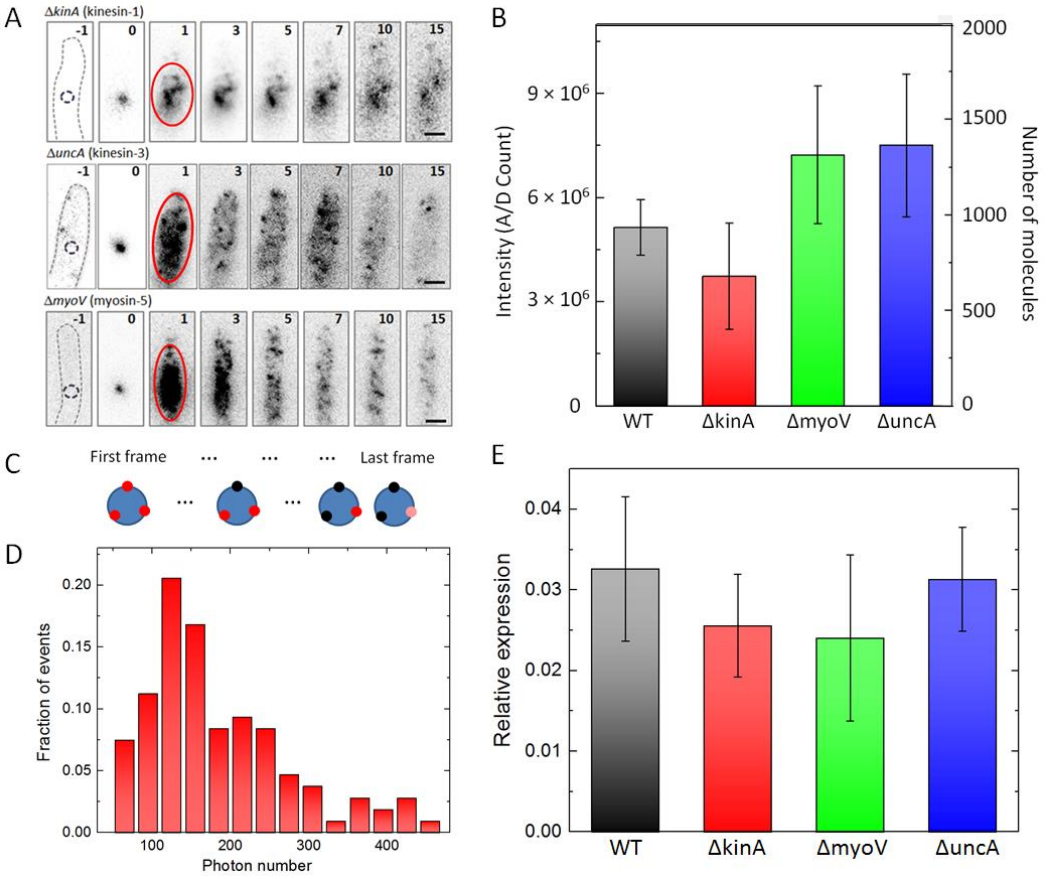

fig. S3. Quantitative analysis of mEosFP*thermo*-ChsB numbers in the hyphal tip and expression levels. (A, B) Intensity-based counting of red-converted fluorescent protein molecules. (A) Selected image sequences of hyphal tips before during and after photoconversion; quantitative analysis was based on the intensities within the local regions marked by red ellipses. (B) Local intensity (left axis) and number of molecules (right axis) for the different cell strains. (C) Schematic of the approach used for detecting single fluorophores: Fluorescent proteins (mEosFP*thermo*) on the same vesicle were gradually bleached, resulting in the detection of single-molecule emission in the last few frames. (D) Distribution of photon numbers from individual mEosFP*thermo* molecules as measured on wildtype cells. (E) Relative expression levels of native *chsB* in the wildtype strain and the motor deletion strains measured by qRT-PCR.

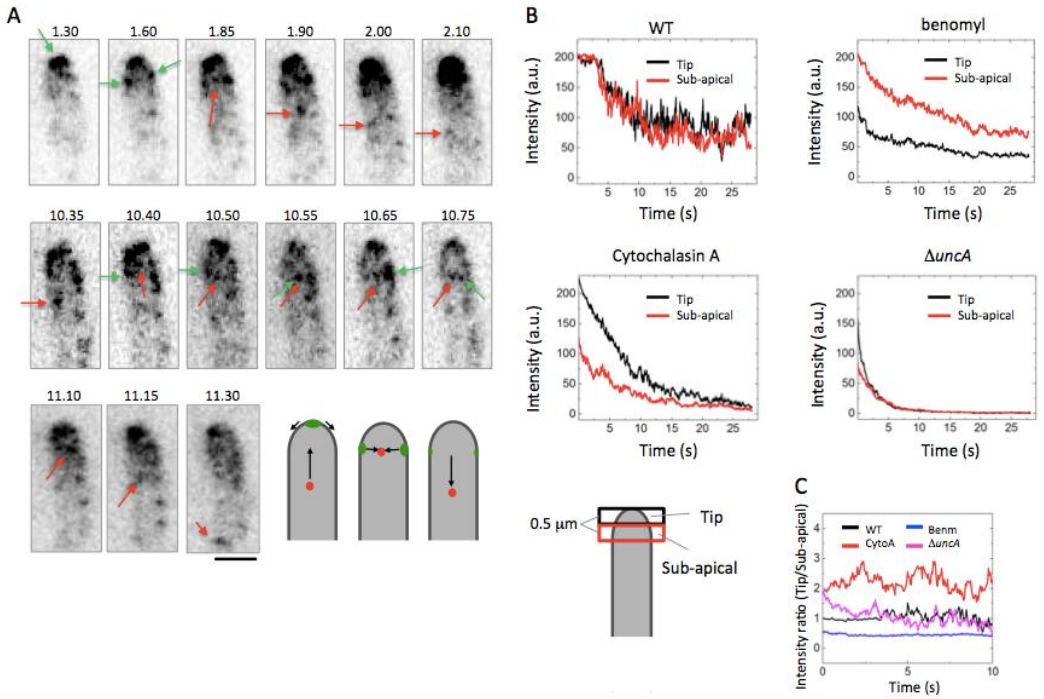

fig. S4. Pulse-chase analysis upon mEosFP*thermo*-ChsB photoconversion at the hyphal tip. (*A*) Three image sequences show ChsB internalization at subapical patches (green arrows) and bi-directional movement (red arrows). The elapsed time is given in seconds. Scale bar, 2 µm. (*B*) Time courses of signal intensity at the hyphal tip regions (black) and subapical regions (red) from the wildtype without and with benomyl or cytochalasin A, and in the *uncA*-deletion strain, and the corresponding intensity ratios between tip and sub-apical regions.

movie S1. Superresolution movie of mEosFP*thermo*-ChsB clusters generated with the moving-window binning technique (500 frames binning with 50 frames shift). Related to Fig. 1A.

movie S2. Dynamics of ChsB clusters identified by cluster analysis. Related to Fig. 1C.

movie S3. Pulse-chase imaging of mEosFP*thermo*-ChsB in the wild-type hyphal tip region with local photoconversion ~5 µm behind the hyphal tip. Related to Fig. 2A.

movie S4. Transport of EEs. Imaging of GFP-RabA movement in a wildtype cell. Related to Fig. S1A.

movie S5. Pulse-chase imaging of mEosFP*thermo*-TeaR in the wild-type hyphal tip region with a local photoconversion ~5 µm behind the hyphal tip. Related to Fig. S1C.

movie S6. Partial comigration of GFP-ChsB and mCherry-RabA. Related to Fig. S1E.

movie S7. Pulse-chase imaging of mEosFP*thermo*-ChsB near the hyphal tip in the presence of microtubule drugs (benomyl, 2 μg/ml). Photoconversion at a spot ~5 μm behind the hyphal tip. Related to Fig. S2C.

movie S8. Pulse-chase imaging of mEosFP*thermo*-ChsB near the hyphal tip in the presence of actin-depolymerizing drugs (cytochalasin A, 2 μg/ml). Photoconversion at a spot ~5 μm behind the hyphal tip. Related to Fig. S2G.

movie S9. Pulse-chase imaging of mEosFP*thermo*-ChsB in the hyphal tip region of the cell from the *kinA* deletion strains. Related to Fig. 3A.

movie S10. Pulse-chase imaging of mEosFP*thermo*-ChsB in the hyphal tip region of the cell from the *uncA* deletion strains. Photoconversion at a spot ~5 μm behind the hyphal tip. Related to Fig. 3B.

movie S11. Pulse-chase imaging of mEosFP*thermo*-ChsB in the hyphal tip region of the cell from the myoV deletion strains. Photoconversion at a spot ~5 μm behind the hyphal tip. Related to Fig. 3C.

movie S12. Pulse-chase imaging after mEosFP*thermo*-ChsB photoconversion at the hyphal tip of a wild-type cell. Related to Fig. 4A.

movie S13. Pulse-chase imaging after mEosFP*thermo*-ChsB photoconversion at the hyphal tip in the presence of microtubule drugs (benomyl, 2 μg/ml). Related to Fig. 4B.

movie S14. Pulse-chase imaging after mEosFP*thermo*-ChsB photoconversion at the hyphal tip in the presence of actin-depolymerizing drugs (cytochalasin A, 2 μg/ml). Related to Fig. 4C.

movie S15. Pulse-chase imaging after mEosFP*thermo*-ChsB photoconversion at the hyphal tip of a cell from the *uncA* deletion strain. Related to Fig. 4D.

table S1. *A. nidulans* strains used in this study.

Strain	Genotype	Source
TN02A3	*pyrG89; argB2; ΔnkuA::argB; pyroA4*	(*51*)
SNR1	*pyrG89; ΔargB::trpΔB; ΔkinA::pyr-4; pyroA4*	(*18*)
SNZ9	*pyrG89; argB2; ΔnkuA::argB; pyroA4; ΔuncA::pyroA*	(*21*)
SRM89	*pyrG89; argB2; ΔnkuA::argB; pyroA4; ΔmyoV::pyrG*	(*49*)
SNT167	*pyrG89; argB2; ΔnkuA::argB; pyroA4; [alcA(p)-mEosthermofp-chsB::pyr-4]*	This study
SNT168	*pyrG89; argB2; ΔnkuA::argB; pyroA4; ΔkinA::pyr-4; [alcA(p)-mEosthermofp-chsB::pyr-4]*	This study
SNT169	*pyrG89; argB2; ΔnkuA::argB; pyroA4; ΔuncA::pyroA; [alcA(p)-mEosthermofp-chsB::pyr-4]*	This study
SNT170	*pyrG89; argB2; ΔnkuA::argB; pyroA4; ΔmyoV::pyrG; [alcA(p)-mEosthermofp-chsB::pyr-4]*	This study
SNT171	*pyrG89; argB2; ΔnkuA::argB; pyroA4; [alcA(p)-gfp-chsB::pyr-4] [alcA(p)-mcherry-rabA::pyroA]*	This study